9

Diffraction Property of Collinear Holographic Storage System

Yeh-Wei Yu and Ching-Cherng Sun
National Central University
Taiwan

1. Introduction

1.1 The collinear volume holographic storage system

The collinear storage system was proposed by Optware [1,2]. It is a coaxially aligned optical structure for signal and reference beams, which are encoded simultaneously by the same spatial light modulator (SLM) and the two beams interfere with each other in the recording medium through a single objective lens. The system has been proven a capability of large storage capacity, high transfer rate, short access time, and besides, it is compatible with existing disc storage systems such as CDs and DVDs [3-4]. Recent report of the collinear Volume holographic storage (VHS) has performed a storage density as high as 270 Gbits/inch^2 [5]. Many advantages are proposed, including uniform shift selectivity in both radial and tangential directions, a fairly large wavelength shift and a fairly large tilt tolerance [6].

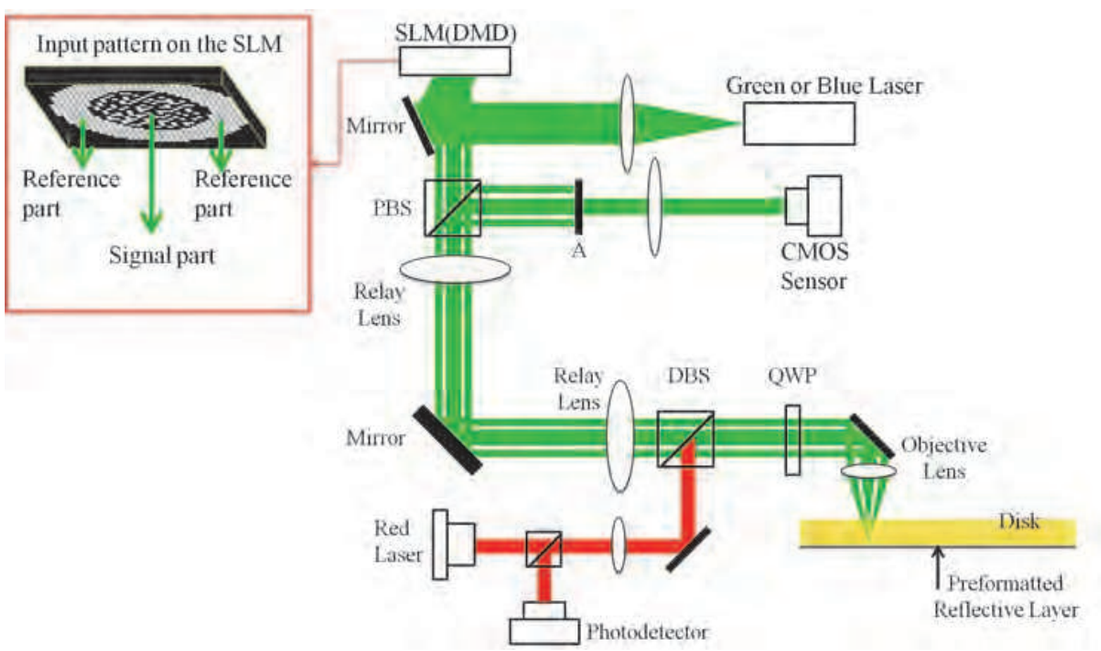

Fig. 1-1. The collinear holographic storage system proposed by Optware [2].

The collinear storage system can be illustrated in Fig. 1-1. Two laser sources are requested in the system, where a red laser is used for the position servor and the green or blue laser is used for data writing and reading. In the writing process, the SLM is imaged on the front focal plane of the objective lens. The central region of the SLM is used to modulate the signal, and the surrounding region of the SLM is used to modulate the reference. After passing through the objective lens, both signal and reference are focused on the reflecting surface of the disk. The interference fringe caused by signal and reference are then recorded by the disk. In the reading process, only the region of the reference beam on the SLM is turn on. The reading beam is then imaged on the front focal plane of the objective lens through the relay lens, and is focused on the reflecting plane of the disc by the objective lens. Then the readout light is diffracted. The reading beams and the diffracted signal are reflected by the reflective layer and re-image on the front focal plane of the objective lens. The combination of quarter wave plate (QWP) and polarization beam splitter (PBS) functions as an isolator, which routes the reflecting diffractive signal and reflecting reading beam to the CMOS sensor. Since the element A blocks reading beams, only diffracted signal can be imaged on the CMOS sensor.

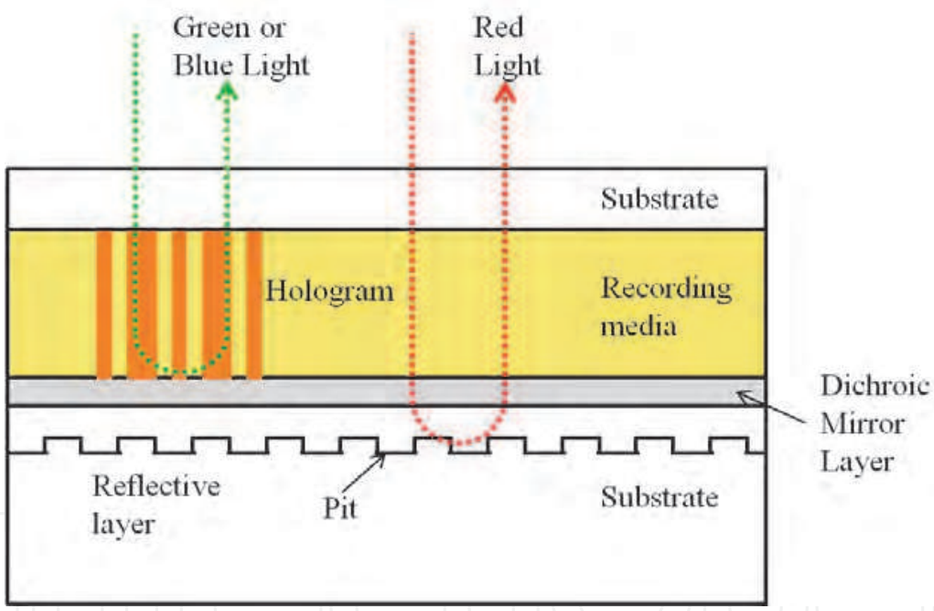

Fig. 1-2. The diagram of the structure of the disc.

The structure of the disc is shown in Fig. 1-2. The dichroic mirror layer reflects the green or blue beam. The red beam propagates through the dichroic mirror layer, and reaches the reflective layer on the substrate. Pits located on the reflective layer induce constructive or destructive interference of the refelected beam. The reflected beam is routed to the photodector, on which the lightness and the darkness can be decoded to do servo-positioning. This system can be simplified as an equivalent model. The two lenses in Fig. 1-3 stand for the objective lens in Fig. 1-2. The collinear system is generally a reflecting architecture, which causes both transparent grating and reflective grating to exist inside the holographic disk. Since the existence of reflective grating decreases the signal to noise ratio (SNR) in the retrieved signal, many techniques are proposed to remove it [7-9]. Accordingly,

only the transparent grating needs to be considered. As shown in Fig. 1-3, the mirror on the back surface of the holographic disk in Fig. 1-2 is replaced by a disc of double-thickness in a modeled transmission algorithm. The two lenses form a 4f system: SLM locates at the front focal plane of the first lens, the disc is located at the back focal plane of the first lens, and the CCD is placed at the back focal plane of the second lens. Fig. 1-3(a) shows the effective model of the writing process. The reference beams from the outer ring of the SLM and the signal beams from the inner circle of the SLM are transformed to frequency domain by the lens and then recorded by the lens. Fig. 1-3(b) shows the effective model of the reading process. Only the light from outer ring can pass through as a reading beam, which is transformed by the lens into frequency domain. Subsequently, the diffracted signal beam and the un-diffracted reading beam are transformed together by the second lens into spatial domain. The aperture blocks the un-diffracted reading beam and leaves only the diffracted signal beam to image on the CCD.

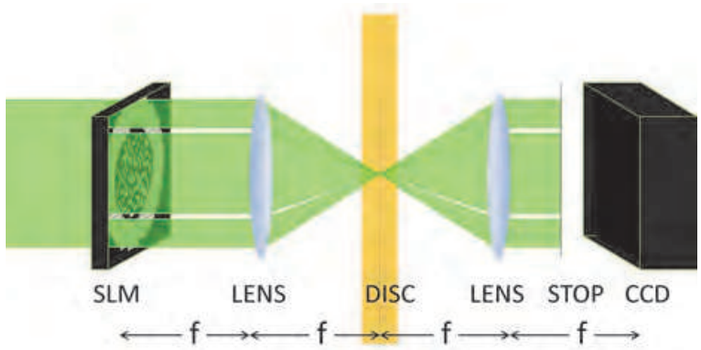

(a)

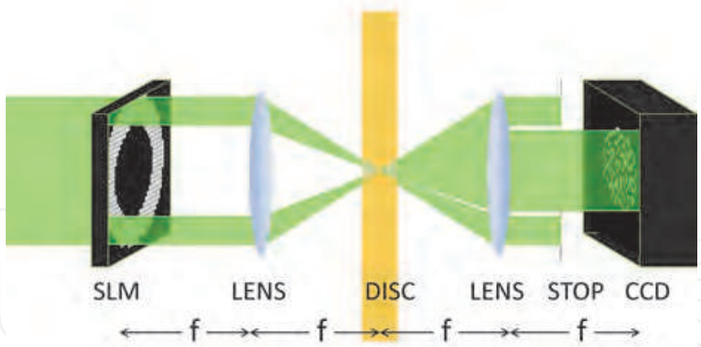

(b)

Fig. 1-3. The simplified model of the coaxial holographic storage system.

1.2 Basic theorem

1.2.1 Two models for the collinear system

In general, the analysis of the VHS system is based on the following two models. The first is to calculate the point spread function (PSF) through Bragg mismatch [10,11]; the second is to apply Fresnel transform to simulate the light field in the recording disc and through Born's approach or the method called "volume hologram being an integrator of the lights emitted from elementary light sources" (VOHIL) to calculate the diffraction

pattern on the CCD plane [12-15]. The procedures of the approaches are described in detaisl from Refs. 10 to Refs.15. For sake of completeness, brief introductions are given here.

For the first model, light from each pixel (*i,j*) on the SLM can be treated as a point light source, it is transferred to a plane wave by the FT lens and is incident on the disk. Thus, the wave vector k_{ij} of the plane wave can be expressed as

$$k_{ij}=\left(-\frac{2\pi}{\lambda}\frac{x_i}{f},-\frac{2\pi}{\lambda}\frac{y_j}{f},\left[\left(n\frac{2\pi}{\lambda}\right)^2-\left(\frac{2\pi}{\lambda}\frac{x_i}{f}\right)^2-\left(\frac{2\pi}{\lambda}\frac{y_j}{f}\right)^2\right]^{1/2}\right), \tag{1-1}$$

where, (x_i, y_j) is the position of the pixel (*i*, *j*). The plane waves from the pixel of information and reference pattern interfere with each other, and reference pattern interfere with each other and is recorded by the media. In the reading process, plane waves from the reference pixels are diffracted by all existing gratings. The diffracted plane waves from the grating can be calculated by coupled mode theory. Considering diffraction of a plane wave from a pixel (*k'*, *l'*) by a grating $K_{klij}=k_{ij}-k_{kl}$, which is written by the interference between the waves from a data pixel (*i, j*) and a reference pixel (*k,l*), the Bragg mismatch is obtained as

$$\Delta k_z=\left(k_{k'l'_z}+K_{klij_z}\right)-\left[\left(nk_0\right)^2-\left(k_{(k'+i-k),(l'+j-l)_x}\right)^2-\left(k_{(k'+i-k),(l'+j-l)_y}\right)^2\right]^{1/2}. \tag{1-2}$$

Thus, the light intensity detected by the CCD is a summation of each pair of plane waves.

For the second model, in the writing process, the optical field in the recording disk can be calculated by Fresnel transform

$$U_{disk}(u,v,\Delta z)=\frac{\exp\left[jk(2f+\Delta z)\right]}{j\lambda^3 f^3}FFT2\left\{U_{SLM}(x,y)\exp\left[-j\frac{\pi\Delta z}{\lambda f^2}\left(x^2+y^2\right)\right]\right\}, \tag{1-3}$$

where, FFT2 is the operator of Fast Fourier Transform in Matlab, which transfers (x, y) into (u/λf, v/λf), U_{SLM} is the signal modulated by the SLM, *x* and *y* are the lateral coordinates of the SLM, *u* and *v* are the lateral coordinates of the recording medium, λ is the wave length, f is the focal length of the lens, and Δz is the distance deviated from the front focal plane of the second FT lens, within the volume of the recording medium. The corresponding intensity distribution is $|U_{disk}|^2$, thus generates an index variation proportional to the intensity distribution. The phase distribution of the medium is then obtained from the index variation.

In the reading process, the optical field of the reading beam can also be calculated by Fresnel transform. The diffracting optical field is obtained by multiplying the recorded phase distribution by the reading beam. Considering the short propagation distance insides the disk, the diffractive optical field propagating to the front focal plane of the second FT lens is calculated by angular spectrum technique

$$U_{df}(u,v,\Delta z) = FFT2\left\{A\left(f_u, f_v, \Delta z\right)\exp\left(\Delta z \cdot 2\pi\sqrt{\frac{1}{\lambda^2} - f_u^2 - f_v^2}\right)\right\}, \tag{1-4}$$

where, U_{df} is the diffractive optical field propagating to the front focal plane of the second FT lens. A is the angular spectrum of the optical field. Therefor, light propagating through the second FT lens and imaging on the CCD can be calculated directly by FFT method. By repeating the above procedures for all layers and summing the calculation results, the final diffractive optical field can be get. Due to the facility of computer calculation, the proposed model can simulate light distribution at any position along the propagation path.

1.2.2 VOHIL theorem

Volume Hologram Being an Integrator of the Lights Emitted from Elementary Light Sources (VOHIL) is a powerful model in calculating the relative diffracting ratio under weak coupling condition [15]. It is used to simplify the optical model. Fig. 1-4 shows an example for calculation by VOHIL theorem. In the writing proces, signal (E_1) and reference (E_2) interfer inside the recording media. The optical field of E_1 and E_2 are expressed

$$E_i = A_i \exp(j\phi_i), \quad i = 1,2, \tag{1-5}$$

where A_j stands for amplitude and ϕ_j stands for phase. The interference fringe is

$$I = \left|A_1\right|^2 + \left|A_2\right|^2 + A_1^* A_2 \exp\left[j(\phi_2 - \phi_1)\right] + A_1 A_2^* \exp\left[j(\phi_1 - \phi_2)\right]. \tag{1-6}$$

Express the reading beam as

$$E_r = A_r \exp\left(j\phi_3\right), \tag{1-7}$$

which is used to probe the media. The diffracted light is

$$D = (\left|A_1\right|^2 + \left|A_2\right|^2)A_r + A_1^* A_2 A_r \exp\left[j(\phi_2 - \phi_1 + \phi_3)\right] + A_1 A_2^* A_r \exp\left[j(\phi_1 - \phi_2 + \phi_3)\right]. \tag{1-8}$$

To detect the diffracted signal on the path of the signal, only the last term need to be considered. So, the diffracting light from each position is

$$D \propto A_r A_2^* A_1 \exp\left[j\phi_1(x_i)\right]\exp\left[j\Delta\phi(x_i)\right], \tag{1-9}$$

where $\Delta\phi(x_i)$ stands for the phase difference at each position, and is

$$\Delta\phi(x_i) = \phi_3(x_i) - \phi_2(x_i), \tag{1-10}$$

the final diffracting light is the integration along the wave propagating direction and can be expressed

$$D \propto \int_{\frac{-t}{2}}^{\frac{t}{2}} A_r A_2^* A_1 \exp\left(j\phi_1\right)\exp\left[j\left(\phi_3 - \phi_2\right)\right]dx, \tag{1-11}$$

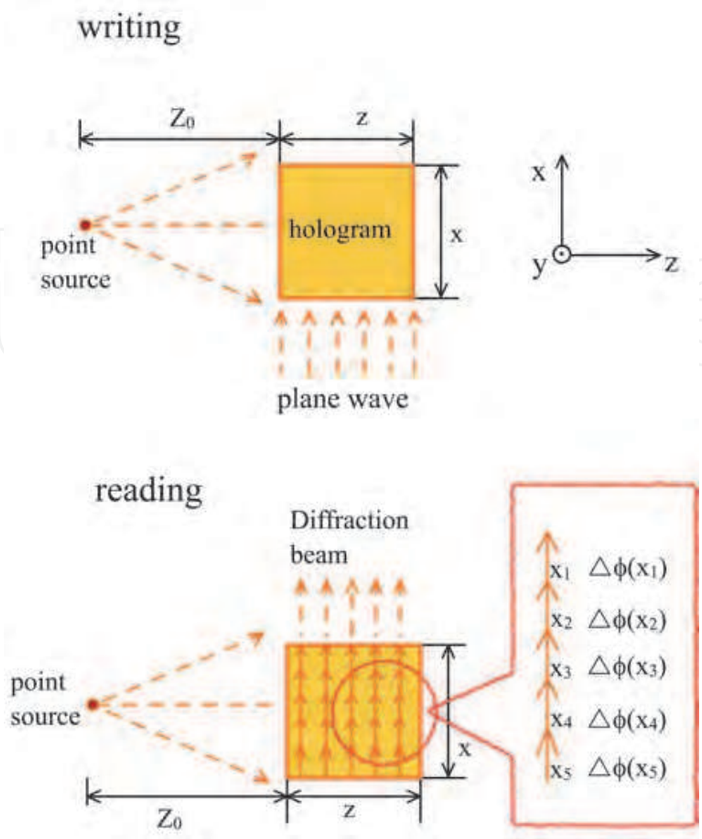

Fig. 1-4. The diagram of VOHIL

where t is the thickness of the recording media along the wave propagating direction. If $\phi_3(x)$ is equal to $\phi_2(x)$, the signal can be perfectly diffracted because of phase match condition. If $\phi_3(x)$ is not equal to $\phi_2(x)$, the phase difference $\Delta\phi(x)$ will be the function of x, the diffractive intensity will be decreased because of phase mismatch. As long as the reading beam is different from the reference in wavelength, incident angle, light source position or other parameters, the diffractive light will be suppressed by phase mismatch. Therefore, Eq. (1-11) can be used to calculate angular selectivity, shift selectivity, wavelength selectivity, temperature tolerance and so on.

In the following paragraph, solutions of collinear system based on VOHIL model are derived out, which clearly point out the physical concepts of the system. Thus, improvement of the system can be proposed based on the physical concepts.

1.3 Point spread function of the system

For volume holographic storage system, both the storage capacity and transfer rate are proportional to the capacity per page. Point spread function (PSF) of the system determines how much data can be stored in one page. If the reference pattern is not well designed, point spread function (PSF) of the collinear system blurs seriously, and thus limits the storage capacity of the system. The radial line (RL) amplitude modulation in reference beam was then proposed to improve the PSF [4]. Even so, 80% of energy is wasted due to the opaque part in the reference region. The random binary phase (RBP) modulation is proposed to

solve this problem, which is shown to improve the PSF without wasting energy in reference modulation [16, 17]. In this section, a novel technique called lens array phase (LAP) modulation is further proposed to improve the PSF.. Thus, the storage capacity and the data transfer rate can be enhanced at the same time.

The effective optical model of collinear system is shown in Fig. 1-3. The optical field of the reference (A_R), signal (A_S) and reading light (A_P) in the disc can be expressed

$$A_R(u,v,\Delta z)=\frac{\exp\left[jk(2f+\Delta z)\right]}{j\lambda f}\Im\left\{U_R(x,y)\exp\left[-j\frac{\pi\Delta z}{\lambda f^2}\left(x^2+y^2\right)\right]\right\}, \tag{1-12}$$

$$A_S(u,v,\Delta z)=\frac{\exp\left[jk(2f+\Delta z)\right]}{j\lambda f}\Im\left\{U_S(x,y)\exp\left[-j\frac{\pi\Delta z}{\lambda f^2}\left(x^2+y^2\right)\right]\right\}, \tag{1-13}$$

$$A_P(u,v,\Delta z)=\frac{\exp\left[jk(2f+\Delta z)\right]}{j\lambda f}\Im\left\{U_P(x,y)\exp\left[-j\frac{\pi\Delta z}{\lambda f^2}\left(x^2+y^2\right)\right]\right\}, \tag{1-14}$$

where U_R, U_S and U_P is the optical field of the reference, signal and probing beams on the SLM, respectively; x and y are the lateral coordinates of the SLM; u and v are the lateral coordinates of the recording medium; $\Im$ stands for Fourier transform which transfers (x, y) into (u/λf, v/λf); k is the wave vector of the light source; λ is the wavelength; f is the focal length of the lens, and Δz is the distance deviated from the focal plane within the volume of the recording medium. The interference of the signal beam and the reference beam can be expressed as

$$I=\left|A_R\right|^2+\left|A_S\right|^2+A_R{A_S}^*+{A_R}^*A_S\,. \tag{1-15}$$

In the reading process, reading beam A_p is used to probe the hologram, and the diffraction is described

$$D=A_p\left(\left|A_R\right|^2+\left|A_S\right|^2\right)+A_pA_R{A_S}^*+A_p{A_R}^*A_S\,. \tag{1-16}$$

In the collinear volume holographic storage system, the dc term is blocked, and the conjugation term is suppressed by deconstruction. So, only the last term need to be considered. Therefore, the optical field diffracted from different layers at a specific depth in the holographic disc is expressed as

$$U(u,v,\Delta z)=\frac{\exp\left[jk(2f+\Delta z)\right]}{j\lambda^3f^3}\left\{\begin{array}{l}\Im\left\{U_P(x,y)\exp\left[-j\frac{\pi\Delta z}{\lambda f^2}\left(x^2+y^2\right)\right]\right\}\\ \Im^*\left\{U_R(x,y)\exp\left[-j\frac{\pi\Delta z}{\lambda f^2}\left(x^2+y^2\right)\right]\right\}\\ \Im\left\{U_S(x,y)\exp\left[-j\frac{\pi\Delta z}{\lambda f^2}\left(x^2+y^2\right)\right]\right\}\end{array}\right\}\Bigg|_{\begin{array}{l}x\to\frac{u}{\lambda f}\\ y\to\frac{v}{\lambda f}\end{array}}. \tag{1-17}$$

The solution for the diffracted optical field in the CCD plane is

$$U_{\det}(\xi,\eta)=\frac{\exp(jk4f)}{(\lambda f)^2}\int_{-T}^{T}\exp\left[\frac{j\pi\Delta z}{\lambda f^2}\left(\xi^2+\eta^2\right)\right]\left\{\begin{array}{l}\left\{U_P(-\xi,-\eta)\exp\left[-j\frac{\pi\Delta z}{\lambda f^2}\left(\xi^2+\eta^2\right)\right]\right\}\\ \otimes\left\{U_R{}^*(\xi,\eta)\exp\left[j\frac{\pi\Delta z}{\lambda f^2}\left(\xi^2+\eta^2\right)\right]\right\}\\ \otimes\left\{U_S(-\xi,-\eta)\exp\left[-j\frac{\pi\Delta z}{\lambda f^2}\left(\xi^2+\eta^2\right)\right]\right\}\end{array}\right\}d\Delta z\,, \tag{1-18}$$

where ⊗ stands for the convolution, ξ and η are the lateral coordinates on the CCD plane, and T is the thickness of the disk. Considering that the probing beam is always the same as the reference beam, and using a point source as the input signal, the PSF can be obtained by calculating the diffracted field on the CCD plane.

$$PSF(\xi,\eta)=\frac{\exp(jk4f)}{(\lambda f)^2}\int_{-T}^{T}\exp\left[\frac{j\pi\Delta z}{\lambda f^2}\left(\xi^2+\eta^2\right)\right]\mathrm{A}COR\{U_R(-\xi,-\eta)\exp[-j\frac{\pi\Delta z}{\lambda f^2}(\xi^2+\eta^2)]\}d\Delta z\,, \tag{1-19}$$

where *ACOR* stands for the autocorrelation. Equation (1-19) shows that the autocorrelation of the reference pattern times a defocusing phase term is dominant in the PSF function.

Four different reference patterns are shown in Fig. 1-5. Eq. (1-19) is applied to simulate the PSF based on the reference patterns, and autocorrelation theorem is used to speed up the simulation [18]

$$ACOR\{O(x,y)\}=IFFT2\{FFT2[O(x,y)]FFT2[O^*(-x,-y)]\}\,, \tag{1-20}$$

where, FFT2 and IFFT2 is the operator of Fast Fourier Transform in Matlab and Inverse Fast Fourier Transform in Matlab, respectively. In the calculation, the thickness is 0.6mm, the wavelength is 532nm and the focal length is 5mm. In order to simplify the effect of the refraction index diference between the air and the holographic disc, the effective focal length is set as 7.5 mm instead of 5 mm, and the effective wavelength is 532 nm/1.5 instead of 532 nm The simulation result of the PSF for the corresponding reference patterns is shown in Fig. 1-6, where λ=532nm, T=0.6mm, pixel size is 13μm×13μm, fill factor of each pixel is 71.6% and the size of the SLM is 4.4mm×4.4mm. The simulation results shows the PSF of the horizontal-line reference pattern is much wider than that of the vertical-line reference pattern along x direction. Similarly, the PSF of the vertical-line reference pattern is also much wider than that of the horizontal-line reference pattern along y direction. Amoung these reference patterns, the radial-line (RL) pattern proposed by Shimura et al. indeed performs a narrower PSF. It is because the RL amplitude modulation avoids the Bragg degeneracy from different pixels in the reference region.

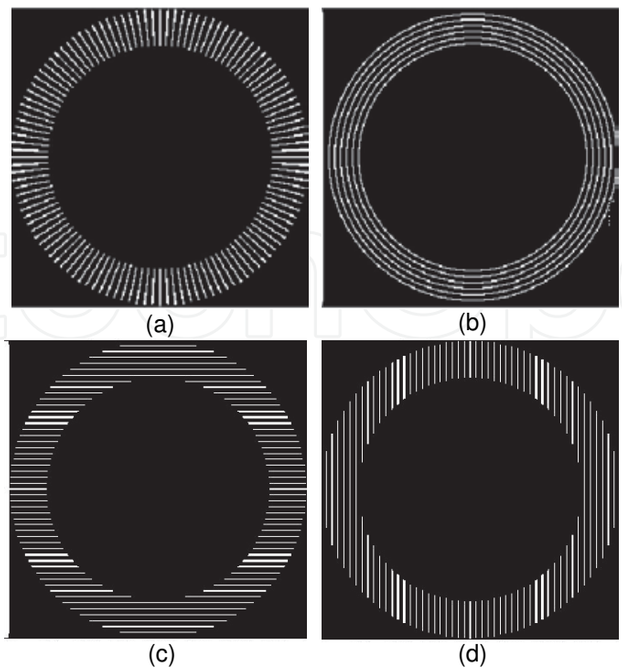

Fig. 1-5. Four different reference patterns. (a) the radial-line (RL), (b) the multi-ring, (c) the horizontal lines and (d) the vertical lines [14].

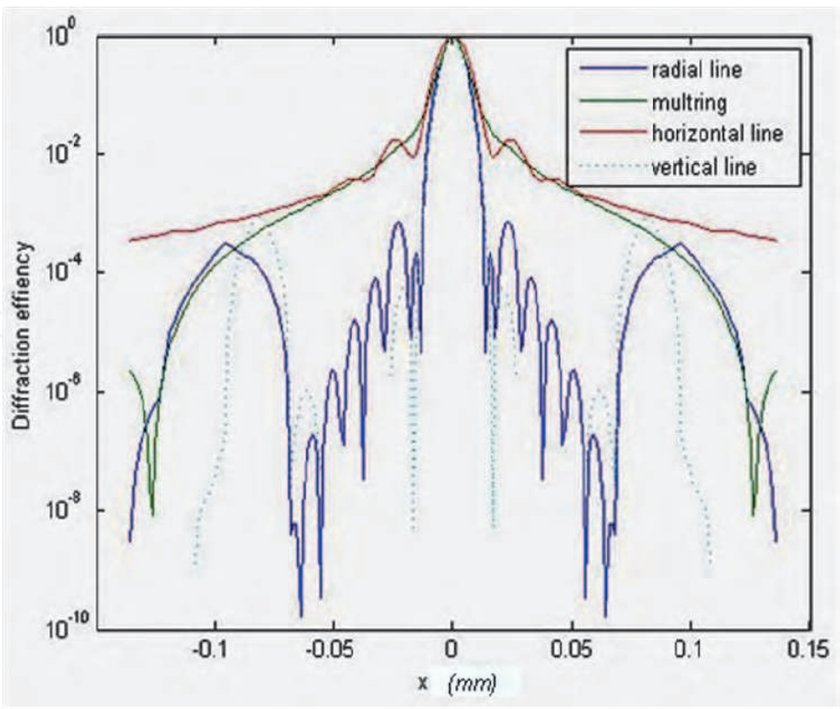

Fig. 1-6. Calculation of intensity of the PSF for the four different reference patterns in Fig. 1-5 [14].

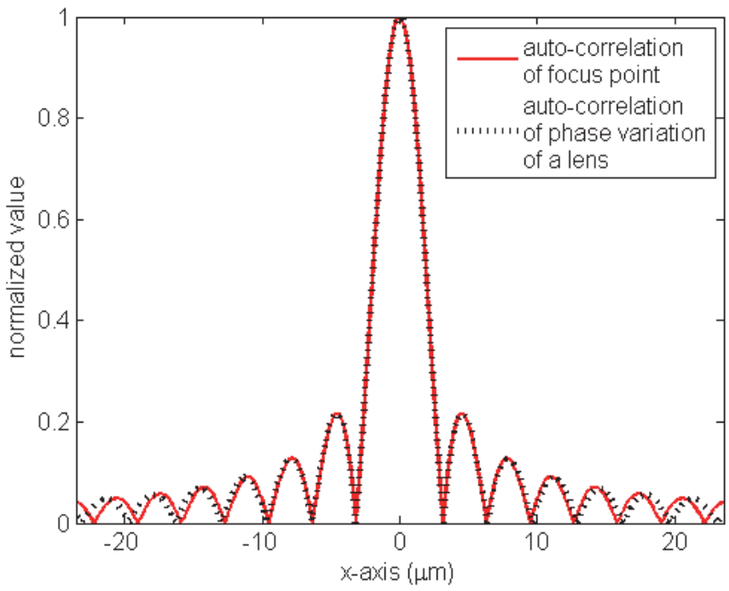

Fig. 1-7. A comparison of the simulation result of the autocorrelation of the phase just behind the lens and at the focal point.

The physical concept described by Eq. (1-19) reveals that the path to achieve the narrowest PSF is through the reference modulation with the narrowest autocorrelation width. Since the autocorrelation of a point source is the sharpest, it looks like the best choice for reference modulation. However, it is not a good policy in the view point of energy. So, a lens array was proposed to approach the effect of point source. The phase modulation of a lens can be described as

$$L(x,y)=\exp\left[-j\pi\left(x^2+y^2\right)/\lambda f_L\right]P(x,y), \tag{1-21}$$

where $P(x,y)$ is the lens pupil, f_L is focal length of the lens. Fig. 1-7 shows a comparison of the autocorrelation of the phase just behind the lens and at the focal point. In the simulation, the focal length f_L is 3.5 mm and the dimensions are 588.24μm×588.24μm. The two curves seem to overlap with each other. Accordingly, lens array phase (LAP) modulation can work as good as points array, and is expressed as

$$LAP(x,y)=\sum_{s=-N}^{N}\sum_{t=-N}^{N}\exp\left[-j\pi\frac{(x-sw)^2+(y-tw)^2}{\lambda f_L}\right]rect\left(\frac{x-sw}{w}\right)rect\left(\frac{y-tw}{w}\right), \tag{1-22}$$

where w is the width of each single lens. Here, the role of the defocusing phase term inside autocorrelation in Eq. (1-19) is ignored, because the phase variation of it is ignorable when comparing with the lens array. Since the width of focus point is related to diffraction limit, the lens array with a higher numeric aperture in each unit lens can provide a tighter PSF.
Figure 1-8 shows three kinds of reference modulation. Fig. 1-8 (a) is the RL modulation with 120 radial lines, where the line width is equal to 13.68μm, Fig. 1-8 (b) is the RBP modulation with pixel pitch equal to 13.68μm and Fig. 1-8 (c) is the LAP modulation with the focal length and area of each single lens equal to 3.5mm and 588.24μm×588.24μm, respectivly. The parameters are choosen with acceptable cut-off frequency and narrowest focus point.

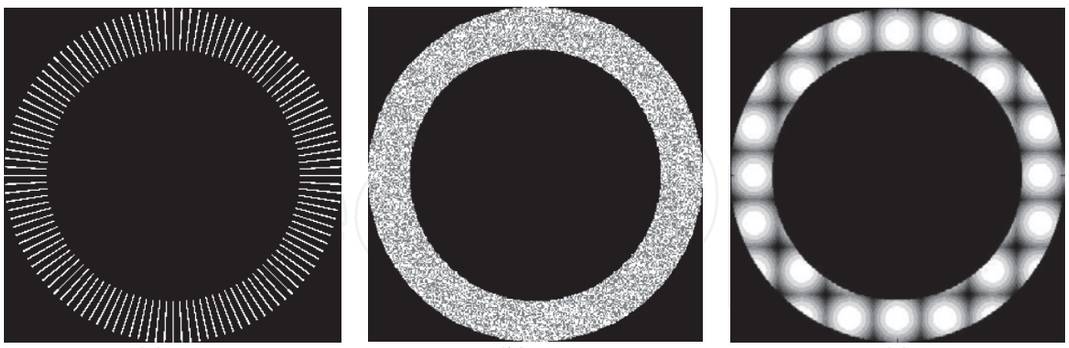

Fig. 1-8. Three kinds of reference modulation: (a) RL modulation; (b) RBP modulation; (c) LAP modulation [19].

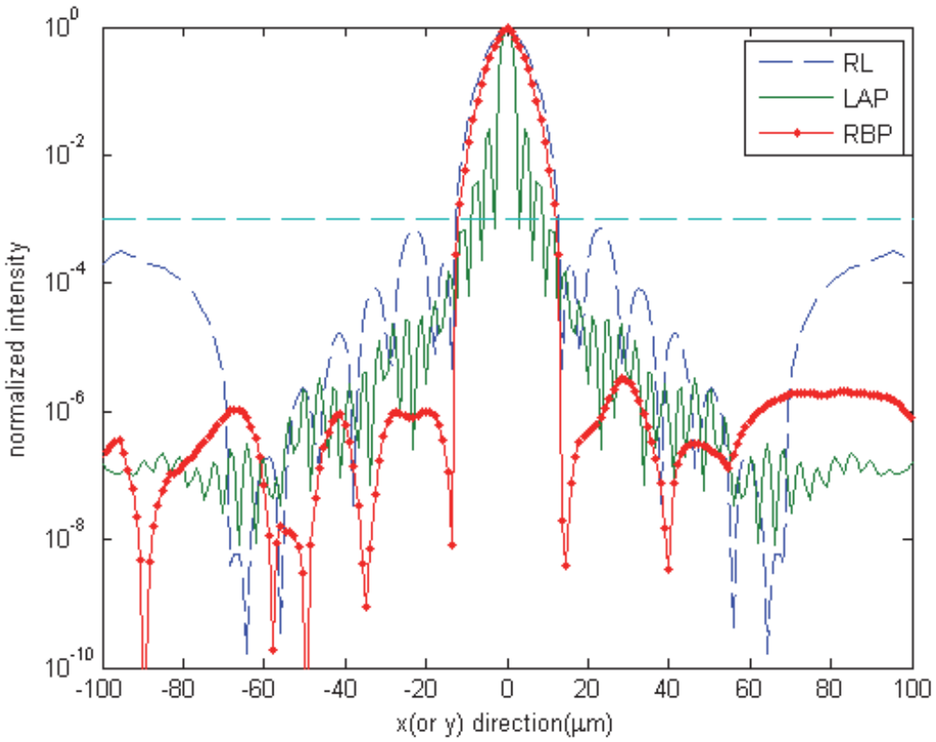

Fig. 1-9. PSF for different reference patterns [19].

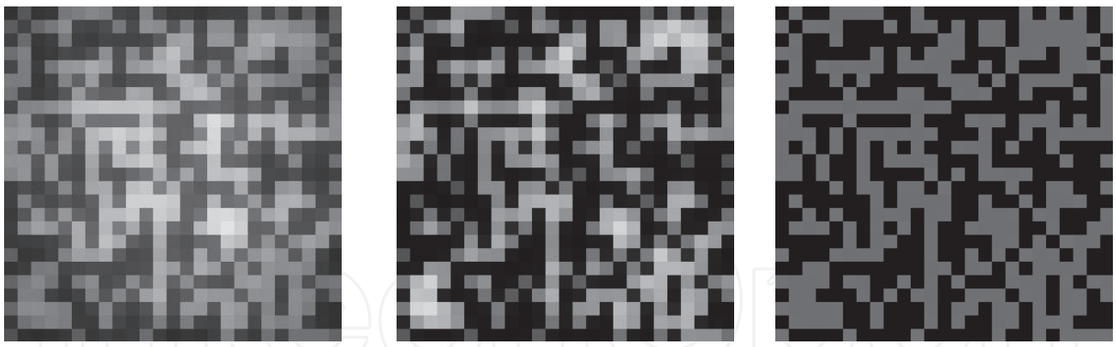

(a) (b) (c)

Fig. 1-10. Simulation result of signal detected by the CCD for (a) RL amplitude modulation, (b) RBP modulation and (c) LAP modulation [19].

Fig. 1-9 is the simulation result of PSF based on Eq. (1-19). It shows that the LAP modulation can tighten the PSF effectively. Fig. 1-10 is the simulated result of the diffracted signal detected by the CCD. The simulation use Eq. (1-18). It shows that the LAP modulation results in the clearest diffracted image with the best readout quality.
The signal to noise ratio (SNR) of the readout pattern is defined as

$$SNR = \frac{(m_1 - m_0)}{\sqrt{\sigma_1^2 + \sigma_0^2}}, \tag{1-23}$$

where σ_0 and σ_1 are the standard deviations of signal 0 and signal 1, respectively ; m_0 and m_1 are the mean values of signal 0 and signal 1, respectively. Eq. (1-23) is used to judge the quality of the diffracted signal. Calculated SNRs for the reference beams with the RL, RBP and LAP modulation are 2.3, 8.1 and 63.2, respectively. The lens array reference with short focal length is shown much helpful in enhancing the SNR of the readout signal of a collinear VHS.

1.4 Shift selectivity of the system

To keep increasing the storage capacity of the collinear VHS, calculation methods for the diffraction property, such as point spread function and shifting selectivity, are highly demanded. It is shown that point spread function is a key issue to calculate the storage capacity of each stored page, and that shifting selectivity is related to the total number of stored pages [20]. In this section, the physics concept of the shifting selectivity for a pixel signal is introduced. Two models of shifting selectivity are proposed. One considering a pixel signal, which is important for precisely describing the shift selectivity. Another model is simplified by considering a point signal as the signal.
The simplified model is based on three assumptions:

1. The shift selectivity is the same for signal point at any position. Therefore, only the center point in the SLM is turned on as signal.
2. In the reading process, the conjugating image point on the CCD plane is dominant. So, only the diffracting intensity at this point is considered.
3. It has been shown that the shift selectivity is independent of the thickness of the disc [21]. Thus, whatever the original thickness of the disk is, the thickness of the disc can always be set as zero.

The shift selectivity of the system is named as "point shift selectivity". The schematic diagram of the storage system for the theoretical model is shown in Fig. 1-3. In the writing process, considering only the center point of the signal, the signal propagating to the disk is a plane wave along z axis, and the grating is expressed

$$R_g^* S_g = \Im\{U_R\}^*, \tag{1-24}$$

where R_g and S_g is the optical field of reference and signal respectively in the medium of the disc. U_R is the optical field of reference in the input plane. The operation $\Im\{\}$ denotes Fourier transform. When the disk shifts, the grating can be expressed

$$G = \Im\{U_R\}^* \otimes \delta(u-\Delta u)\delta(v-\Delta v), \tag{1-25}$$

where (u,v) is the coordinate of the disk, Δu and Δv is the shifting of the disk in the u direction and v direction respectively. When a probing beam is used to read the disk, the diffracted light can be expressed

$$U_d = \Im\{U_P\}\Big|_{\substack{u/(\lambda f)\\ v/(\lambda f)}} \Im\{U_R\}^*\Big|_{\substack{(u-\Delta u)/(\lambda f)\\ (v-\Delta v)/(\lambda f)}}, \tag{1-26}$$

where U_P is the optical field of the probing beam in the input plane. Let the probing beam be the same as the reference beam, the diffracted optical field at the conjugating image point on the CCD plane can be expressed

$$\begin{aligned} U(\Delta u,\Delta v) &= \iint \Im\{U_P\}\Big|_{\substack{u/(\lambda f)\\ v/(\lambda f)}} \Im\{U_R\}^*\Big|_{\substack{(u-\Delta u)/(\lambda f)\\ (v-\Delta v)/(\lambda f)}} \exp\left[-\frac{2\pi j}{\lambda f}(u\xi+v\eta)\right] du dv\Big|_{\substack{\xi=0\\ \eta=0}}, \\ &= \Im\left\{|U_R|^2\right\}\Big|_{\substack{\Delta u/(\lambda f)\\ \Delta v/(\lambda f)}} \end{aligned} \tag{1-27}$$

where (ξ,η) is the coordinate of the CCD plane. Thus, the diffracted intensity depending on disk deviation can simply be expressed

$$I(\Delta u,\Delta v) = \left|\Im\left\{|U_R|^2\right\}\Big|_{\substack{\Delta u/(\lambda f)\\ \Delta v/(\lambda f)}}\right|^2. \tag{1-28}$$

Thus, the point shifting selectivity equals to square of Fourier transform of intensity distribution of the reference pattern.

Fig. 1-11 shows five different reference patterns. Fig. 1-11 (a) is a ring pattern with phase modulation of $\exp[j2\pi\cos(y/\Lambda)]$. Fig. 1-11 (b) is a ring pattern with amplitude modulation of $\cos(y/\Lambda)$. Where $\Lambda/2\pi$ is the period of the cosine function and is equal to 273.6μm. Fig. 1-11 (c) is a ring pattern with random binary amplitude modulation, and the pixel size is 13.68μm×13.68μm. Fig. 1-11 (d) is random phase modulation in a ring pattern, where the modulation pitch is 13.68μm×13.68μm. Fig. 1-11 (e) is a ring pattern without any modulation inside. In the simulation, the wavelength is 408nm; the focal length of the objective lens is 4mm.

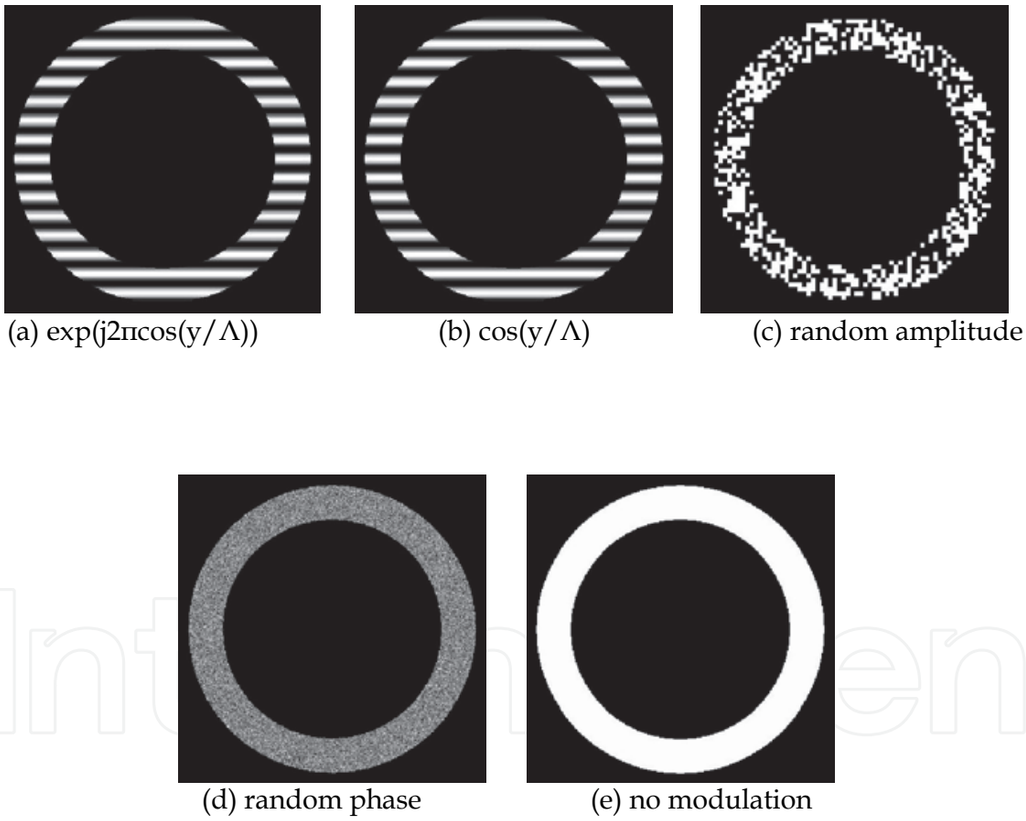

(a) $\exp(j2\pi\cos(y/\Lambda))$ (b) $\cos(y/\Lambda)$ (c) random amplitude

(d) random phase (e) no modulation

Fig. 1-11. The reference patterns used in the simulation [22].

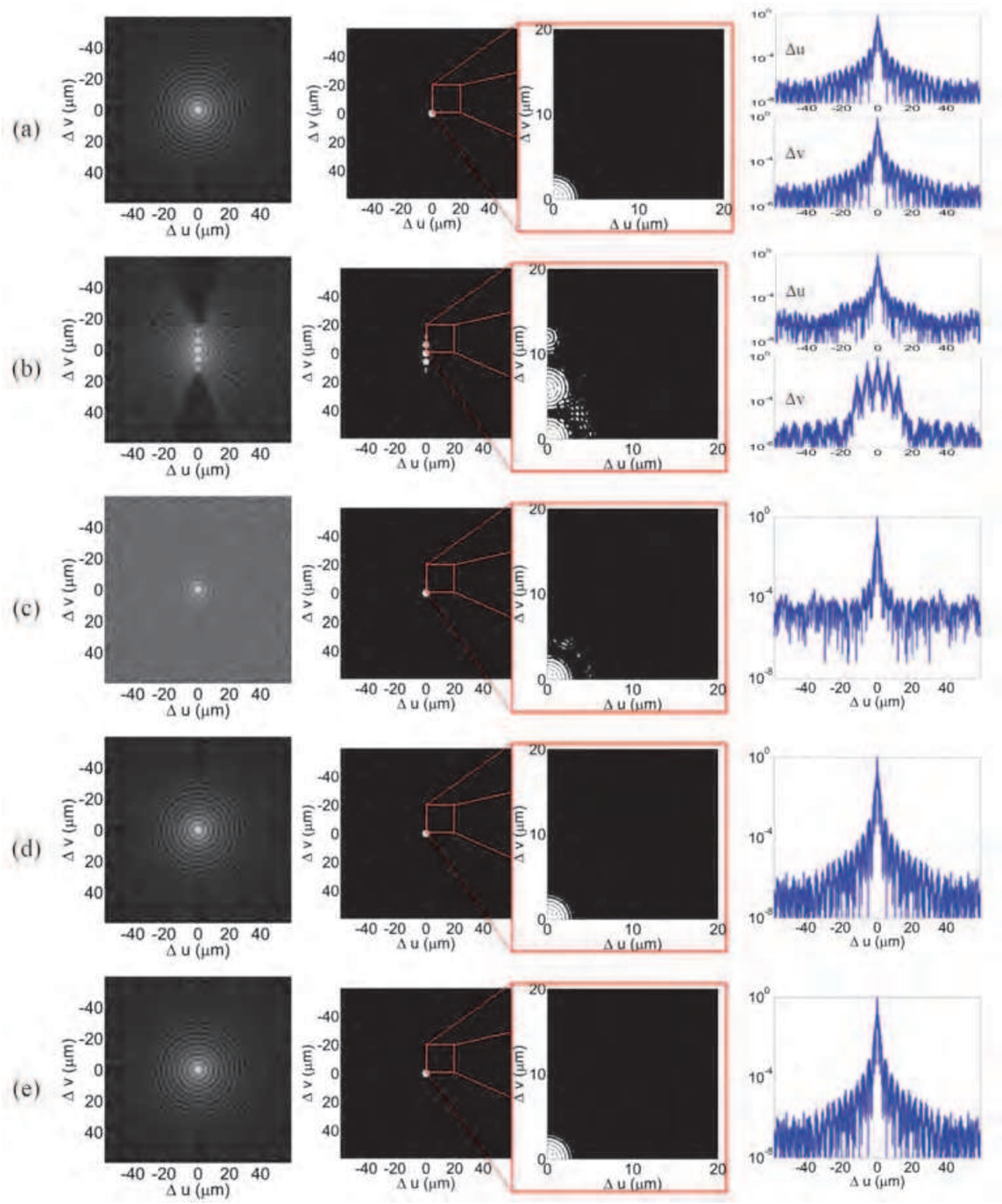

Fig. 1-12. The simulation result of the point shifting selectivity, based on Eq. (1-28), for a point located at the center of the signal plane corresponding to the reference patterns in Fig. 1-11. The figures from left to right are followed with 2-D shifting selectivity, 2-D shifting selectivity after thresholding and its enlarged pattern, 1-D shifting selectivity [22].

Fig. 1-12 (a)~(e) show a simulation of point shifting selectivity corresponding to the reference patterns shown in Fig. 1-11 (a)~(e). The simulation uses Eq. (1-28) and Fast Fourier Transform in Matlab for fast calculation. Figures in the first columns are 2-D shift selectivity, where the horizontal and vertical axes correspond to the shifting along Δu and Δv, respectively. The grey level in each point represents the diffraction intensity (in log scale) collected by the corresponding image point of the CCD. To emphasize cross-talk caused by the 2-D shifting selectivity, a threshold value of 10^{-3} is used in the second column. Each white point stands for the intensity larger than the threshold value, and black point stands for the intensity below the value. Figures in the last column show the 1-D shift selectivity. It is shown that the point shift selectivity shown in Fig. 1-12 (a), Fig. 1-12 (d) and Fig. 1-12 (e) are all the same. Obviously, the point shift selectivity cannot tell the effect of the phase modulated reference patterns. Even so, the simple relationship still provides a simple prediction rule for designing reference pattern.

For a precise calculation, a more complicated model should be adopted. The model named "pixel shift selectivity" does not use the three assumptions in point shift selectivity. It considers the response of one pixel to simulate the real condition. Inside the disk, the optical field of the reference (A_R), signal (A_S) and reading light (A_P) have been described in Eq. (1-12), Eq. (1-13) and Eq. (1-14). When the disk shifts, based on VOHIL model, the optical field diffracted from specific layer at a depth (Δz) can be expressed

$$U(u-\Delta u, v-\Delta v, \Delta z) = \frac{\exp\left[jk(2f+\Delta z)\right]}{j\lambda^3 f^3} \Im\left\{U_P(x,y)\exp\left[-j\frac{\pi\Delta z}{\lambda f^2}\left(x^2+y^2\right)\right]\right\} \times \left\{\delta(u-\Delta u, v-\Delta v) \otimes \left\{\begin{array}{l} \Im^*\left\{U_R(x,y)\exp\left[-j\frac{\pi\Delta z}{\lambda f^2}\left(x^2+y^2\right)\right]\right\} \\ \Im\left\{U_S(x,y)\exp\left[-j\frac{\pi\Delta z}{\lambda f^2}\left(x^2+y^2\right)\right]\right\} \end{array}\right\}\right\}. \quad (1\text{-}29)$$

The optical field is thus propagating to the CCD plane and is integrated along Δz.

$$U_{\det}(\xi,\eta,\Delta u,\Delta v) = \frac{2T\exp(4jkf)}{(\lambda f)^2} \int_{-\infty}^{\infty}\int_{-\infty}^{\infty} \Im\left\{\begin{array}{l} U_p\left(\xi_2-\xi,\eta_2-\eta\right)U_R{}^*\left(\xi_2+\xi_1,\eta_2+\eta_1\right) \\ \sin c\left[-2T\frac{\xi_2\left(\xi_1+\xi\right)+\eta_2\left(\eta_1+\eta\right)}{\lambda f^2}\right] \end{array}\right\} \Bigg|_{\frac{\Delta v}{\lambda f}}^{\frac{\Delta u}{\lambda f}} U_S(\xi_1,\eta_1)d\xi_1 d\eta_1, \quad (1\text{-}30)$$

where, T is the thickness of the recording media, (ξ, η) is the coordinate on the output CCD plane, (ξ_1 ,η_1) is the coordinate on the input SLM plane, and (ξ_2, η_2) is the parameter caused by convolution. Considering a pixel in the center of the SLM as the signal and integrating the intensity of the whole pixel in the center of the CCD, the pixel shift selectivity is

$$I_{pixel}(\Delta u,\Delta v)=$$

$$\iint_{\text{pixel}}\left|\iint_{pixel}\Im\left\{\begin{matrix}U_P(\xi_2-\xi,\eta_2-\eta)U_R{}^{*}(\xi_2+\xi_1,\eta_2+\eta_1)\\ \sin c\left[-2T\dfrac{\xi_2(\xi_1+\xi)+\eta_2(\eta_1+\eta)}{\lambda f^2}\right]\end{matrix}\right\}\Bigg|_{\substack{\frac{\Delta u}{\lambda f}\\ \frac{\Delta v}{\lambda f}}}d\xi_1 d\eta_1\right|^2 d\xi d\eta\,. \tag{1-31}$$

Eq. (1-31) shows that the shifting selectivity is nearly the autocorrelation of the Fourier transform of the reference pattern, and is independent of thickness as long as (ξ, η) is close to ($-\xi_1$,$-\eta_1$). This condition can always be satisfied when the diffracting signal locates near the conjugate image position. Thus, the broader reference pattern will cause narrower Fourier transform pattern. Fig. 1-13 shows the 2-D pixel shifting selectivity. It is find the first two patterns perform relative higher shifting selectivity in one direction. The reason is the Fourier transform pattern of the reference pattern is narrower in the direction. For the ring patterns in random phase or amplitude modulation, there seems no obvious difference. Among all these patterns, the ring pattern without any modulation shows the best shifting selectivity because the Fourier transform pattern of the last one is the narrowest.

The simulation result in Fig. 1-13 shows that the reference pattern is important to the shifting selectivity. But, as mentioned in Section 1.3, the reference pattern is also important to the PSF. Fig. 1-14 shows the simulated 1-D PSF for the five patterns shown in Fig. 1-11. Actually, to design an appropriate reference pattern to simultaneously obtain narrower PSF and higher shifting selectivity is one of the most important issues in a collinear system.

1.5 Summary

In this chapter, the collinear holographic storage system is studied. An effective model is used to analyze the system. Based on Fresnel transform and the VOHIL model, paraxial solutions to describe the diffraction characteristic of the collinear holographic system are carried out. The solutions are used to figure out the the physics insight of the system. In Eq. (1-19), it shows that the PSF is related to the auto-correlation function of the reference pattern times a defocusing phase term. Accordingly, a lens array used as the reference is introduced. From the simulated diffracted signal on the CCD plane, the SNR for LAP modulation can be obtained as high as 63.2, which is much larger than 2.3 in RL reference and 8.1 in RBP reference. Besides, the discussed physics concept is important in designing a more effective VHS system when other system characteristics such like system tolerance are taken into consideration.

Equation (1-28) based on a simplified model shows point shifting selectivity is related to Fourier transform of intensity distribution of the reference pattern. It provides a simple prediction rule for designing some reference patterns to improve the shift selectivity of the system. The equation shows that the broader the reference pattern is, the higher shifting selectivity we get. To obtain an accurate calculation, Eq. (1-31) is derived out without using the three assumptions in point shift selectivity, and the result is called pixel shift selectivity. It

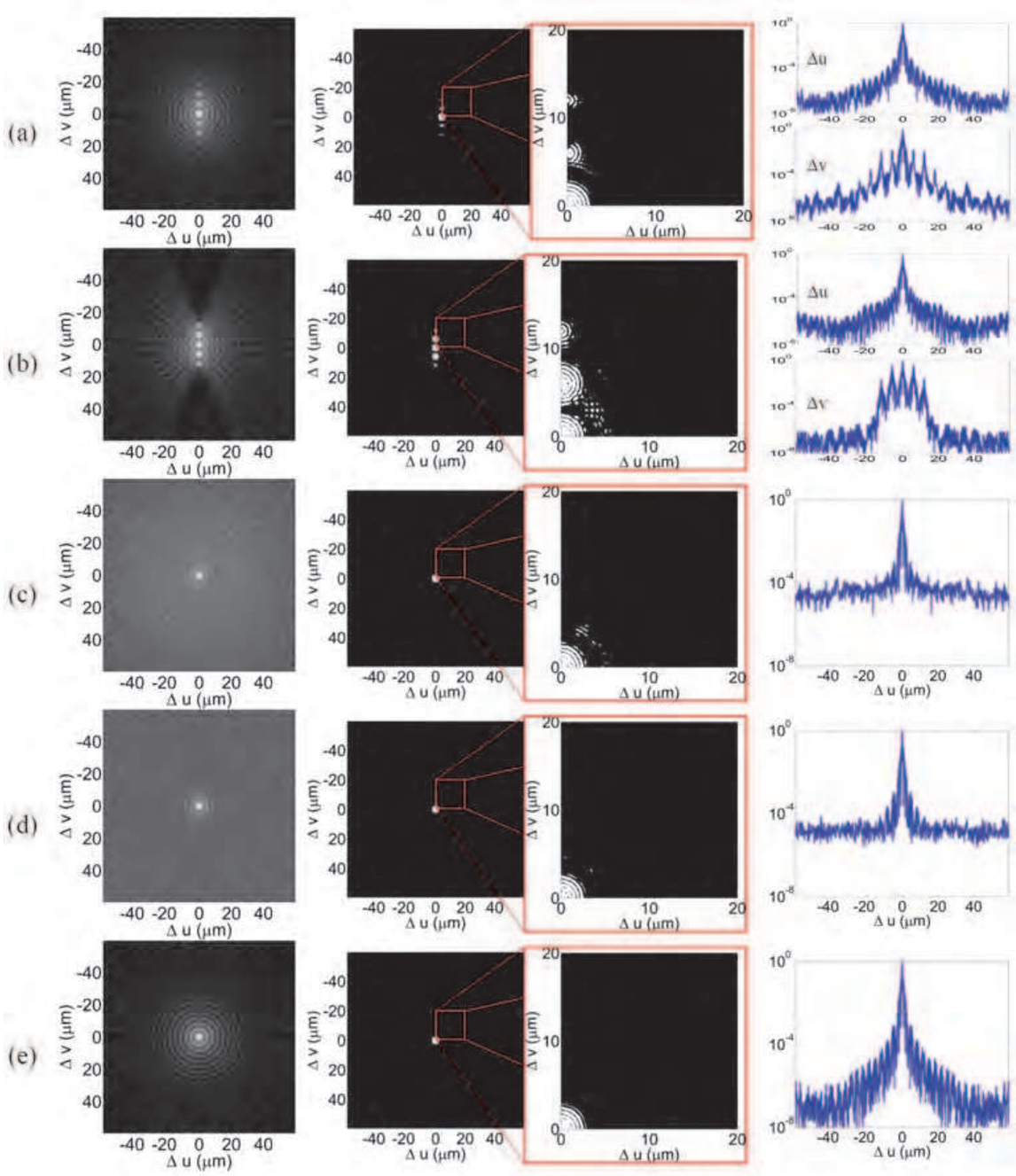

Fig. 1-13. The simulation result of the shifting selectivity for a pixel located at the center of the signal plane corresponding to the reference patterns in Fig. 11. The figures from left to right are followed with 2-D shifting selectivity, 2-D shifting selectivity after thresholding and its enlarged pattern, 1-D shifting selectivity [22].

shows that the shifting selectivity is nearly an autocorrelation of the Fourier transform of the reference pattern, and is independent of thickness of the recording medium when the diffracting signal is located near the conjugate image position. The simulation results shows both amplitude and phase modulation make no obvious change in shifting selectivity, so shifting selectivity is not affected through advanced design of reference pattern. The solution will be useful in the design of a reference pattern to perform high-quality readout in the collinear holographic storage system.

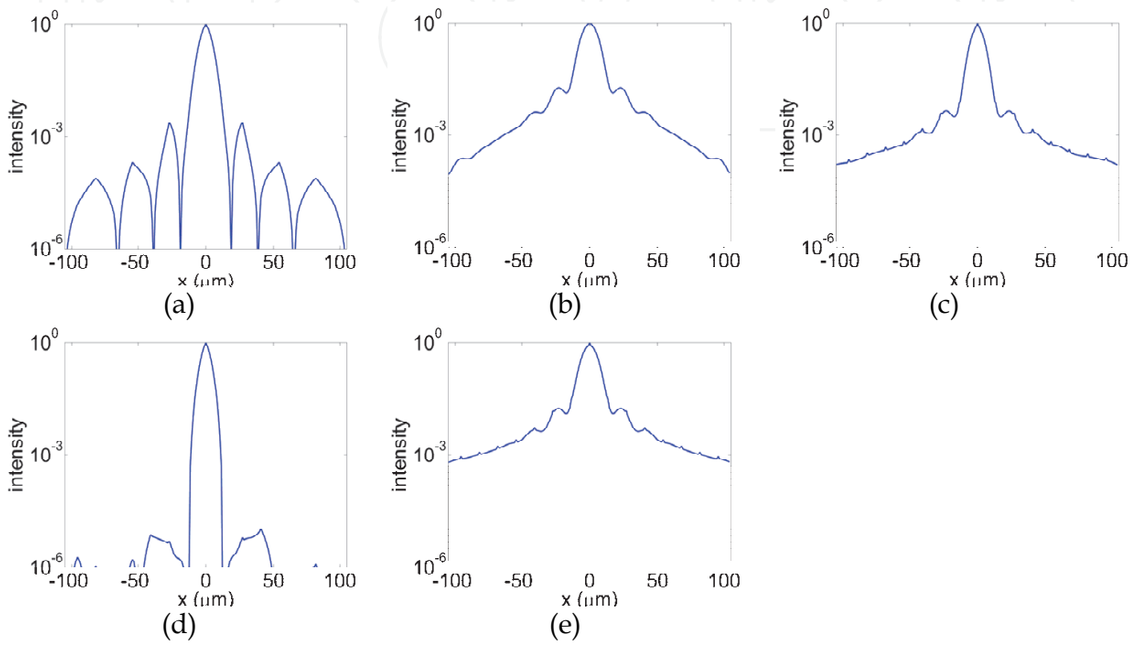

Fig. 1-14. The simulation result of the impulse response for a point located at the center of the signal plane corresponding to the reference patterns in Fig. 11 [22].

2. References

[1] H. Horimai, "Collinear Holography", The 5th Pacific Rim Conference on Lasers and Electro-Optics, Proceedings 1, Taiwan, (2003).

[2] H. Horimai and L. Jun, "A Novel Collinear Optical Setup for Holographic Data Storage System", Proc. of SPIE 5380, 297-303 (2004).

[3] H. Horimai and X. Tan, "Advanced collinear holography," Opt. Rev. 12, 90–92 (2005).

[4] H. Horimai, X. D. Tan, and J. Li, "Collinear holography," Appl. Opt. 44, 2575–2579 (2005).

[5] K. Tanaka, H. Mori, M. Hara, K. Hirooka, A. Fukumoto, and K. Watanabe, "High density recording of 270 Gbits/inch2 in a coaxial holographic storage system," Tech. Digest of ISOM 2007, MO–D–03.

[6] H. Horimai and X. Tan, "Holographic versatile disc system," Proc. of SPIE 5939, 593901(2005).

[7] M. Toishi, "Holographic recording and reconstructing apparatus and holographic recording and reconstructing method," United States Patent Application Publication, US 20060176532 A1 (2006).

[8] B. King, K. Anderson and K. Curtis, "System and method for reflective holographic storage with associated multiplexing technique," United States Patent, US 6721076 B2 (2004).
[9] H. Horimai, Y. Sakane and K. Kimura, "Optical information-recording medium, optical information recording apparatus and optical information reproducing apparatus including optical information-recording medium and method for manufacturing polarization changing layer," United States Patent, US2004/0165518 A1 (2004).
[10] T. Shimura, S. Ichimura, R. Fujimura, K. Kuroda, X. D. Tan and H. Horimai, "Analysis of a collinear holographic storage system: introduction of pixel spread function," Opt. Letters 31, 1208–1210 (2006).
[11] X. Tan and H. Horimai, "Collinear™ technology for holographic versatile disc (HVD™) system," Proc. of SPIE 6343, 63432w (2006).
[12] H. Horimai and X. Tan, "Advanced collinear holography," Opt. Rev. 12, 90–92 (2005).
[13] S. R. Lambourdiere, A. Fukumoto, K. Tanaka, and K. Watanabe, "Simulation of holographic data storage for the optical collinear system," Jpn. J. Appl. Phys. 45, 1246–1252 (2006).
[14] C. C. Sun, Y. W. Yu, S. C. Hsieh, T. C. Teng and M. F. Tsai "Point spread function of a collinear holographic storage system," Optics Express 15, 18111-18118 (2007).
[15] C. C. Sun, "A simplified model for diffraction analysis of volume holograms," Opt. Eng. 42, 1184–1185 (2003).
[16] K. Tanaka, M. Hara, K. Tokuyama, K. Hirooka, K. Ishioka, A. Fukumoto and K. Watanabe, "Improved performance in coaxial holographic data recording," Optics Express 15, 16196-16209 (2007).
[17] C. B. Burckhardt, "Use of a random phase mask for the recording Fourier transform holograms of data masks," Appl. Opt. 9, 695–700 (1970).
[18] J. W. Goodman, *Introduction to Fourier Optics* (McGraw-Hill, 2002).
[19] Y. W. Yu, C. Y. Cheng, and C. C. Sun, "Increase of signal-to-noise ratio of a collinear holographic storage system with reference modulated by a ring lens array," Opt. Lett. 35, 1130-1132 (2010).
[20] T.Shimura, Y. Ashizuka, M. Terada, R. Fujimura, and K. Kuroda, "What Limits the Storage Density of the Collinear Holographic Memory," Tech. Digest of 32 ODS2007,TuD1.
[21] T. Shimura, S. Ichimura, Y. Ashizuka, R. Fujimura, K. Kuroda, X. D. Tan, and H. Horimai, "Shift selectivity of the collinear holographic storage system," Proc. of 35 SPIE 6282, 62820s (2006).
[22] Y. W. Yu, T. C. Teng, S. C. Hsieh, C. Y. Cheng, and C. C. Sun, "Shifting selectivity of collinear volume holographic storage," Opt. Comm.283, 3895-3900 (2010).

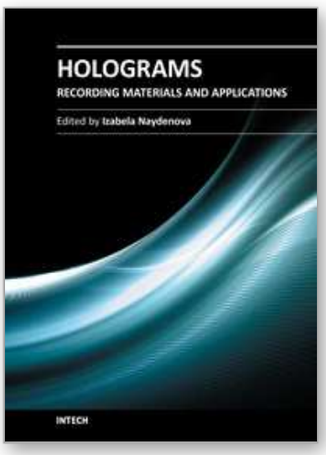

Holograms - Recording Materials and Applications

Edited by Dr Izabela Naydenova

ISBN 978-953-307-981-3
Hard cover, 382 pages
Publisher InTech
Published online 09, November, 2011
Published in print edition November, 2011

Holograms - Recording Materials and Applications covers recent advances in the development of a broad range of holographic recording materials including ionic liquids in photopolymerisable materials, azo-dye containing materials, porous glass and polymer composites, amorphous chalcogenide films, Norland optical adhesive as holographic recording material and organic photochromic materials. In depth analysis of collinear holographic data storage and polychromatic reconstruction for volume holographic memory are included. Novel holographic devices, as well as application of holograms in security and signal processing are covered. Each chapter provides a comprehensive introduction to a specific topic, with a survey of developments to date.

InTech Europe
University Campus STeP Ri
Slavka Krautzeka 83/A
51000 Rijeka, Croatia
Phone: +385 (51) 770 447
Fax: +385 (51) 686 166
www.intechopen.com

InTech China
Unit 405, Office Block, Hotel Equatorial Shanghai
No.65, Yan An Road (West), Shanghai, 200040, China
中国上海市延安西路65号上海国际贵都大饭店办公楼405单元
Phone: +86-21-62489820
Fax: +86-21-62489821

IntechOpen